

ORIGINAL RESEARCH ARTICLE

Open Access



The effects of saline water preheating and heat recovery in a vapour-based multistage solar still

Mfanafuthi Mthandeni Mkhize^{1*}  and Velaphi Msomi¹

Abstract

The current study complements a broader body of research on solar distillation, including research on heat recycling capabilities and other related factors in multistage solar distillation systems. Solar stills can be used in various applications to provide safe and clean water from natural sources. This study is based on field data collected, analysed, and interpreted over ten (10) months. The solar still operated at atmospheric pressure and produced a distillate by evaporating saline water (SW) at ~ 100 °C. The maximum SW preheating was 75.5 °C with 30,821.04 kJ/m² day collected by the solar collectors. The corresponding overall thermal efficiency of the test rig was 33.83%. The overall thermal efficiency decreased with increasing wind speed, averaging at 3.12 m/s to 28.31% due to increased heat loss to the environment when 30,780 kJ/m²day was collected. It further declined to 5.89% with low meteorological conditions of 209.81 W/m², 15.66 °C and 2.66 m/s, respectively, on average. However, the benefits of increased wind speed were enhanced condensation and productivity. The study also found that the ideal thermal energy delivery rate was ~ 600 W/m² or an impulsive mode at higher solar insolation. A balanced condensation rate, SW preheating, heat recovery and overall thermal efficiency can be achieved at this delivery rate. A significant correlation was observed, indicating that the simultaneous increase in the average heat input rate and wind velocities positively impacted distillate output. Conversely, low average wind velocity improved overall thermal efficiency, resulting in a distillate output of 6730 ml for the five stacked stages, despite a slight discrepancy of 3.2 W/m² in the heat input rate.

Keywords Thermal efficiency, Preheating, Heat recovery, Multistage, Thermal inertia, Solar energy

Introduction

Using the concept of heat recycling to improve system performance is well-known in engineering applications and has been around for some time. A solar still is a renewable energy engineering device that desalinate brackish water through thermal energy. However, solar stills generally cannot complete the evaporation and condensation cycle without environmental influence (wind,

solar irradiance, ambient temperature, etc.) that can be positive, negative, or minimal. For example, solar stills produce negligible distillate at low solar insolation and ambient air temperatures (Özcan & Deniz, 2023).

Some studies reported a limited effect of wind speed on solar energy devices, while others found wind speed effective. However, combining heat recovery and SW preheating can significantly improve the operation of solar stills. For example, SW preheating increases the feed-water temperature at the inlet to the solar still, regardless of heat losses. Heat recovery, on the other hand, is to recover as much of the latent heat of condensation as possible, thereby improving the efficiency of the solar distiller (Abd Elbar & Hassan, 2020; Mdletshe et al., 2023; Pangwa & Msomi, 2022).

*Correspondence:

Mfanafuthi Mthandeni Mkhize
sggamkhize@gmail.com

¹ Mechanical and Mechatronic Engineering Department, Faculty of Engineering and the Built Environment, Cape Peninsula University of Technology, P.O. Box 1906, Bellville 7535, South Africa



© The Author(s) 2023. **Open Access** This article is licensed under a Creative Commons Attribution 4.0 International License, which permits use, sharing, adaptation, distribution and reproduction in any medium or format, as long as you give appropriate credit to the original author(s) and the source, provide a link to the Creative Commons licence, and indicate if changes were made. The images or other third party material in this article are included in the article's Creative Commons licence, unless indicated otherwise in a credit line to the material. If material is not included in the article's Creative Commons licence and your intended use is not permitted by statutory regulation or exceeds the permitted use, you will need to obtain permission directly from the copyright holder. To view a copy of this licence, visit <http://creativecommons.org/licenses/by/4.0/>.

Therefore, many pioneering external features, such as phase change materials (PCMs), have improved solar still productivity (Khalilmoghadam et al., 2021). However, the performance of solar stills can be further enhanced by SW preheating and heat recovery by changing its geometry and flow configuration (Zhu et al., 2022). In addition, integrating additional or external functions to increase solar still productivity can result in high operating costs. Therefore, it is a priority to fully reuse the heat produced by the distiller before adding external sources (Aboabboud et al., 1997). Chen et al. (2023) report that energy savings of up to 6720.68 kJ/day by integrating SW preheating and heat recovery into the desalination system is possible. Furthermore, preheating the SW to a maximum temperature of 61.3 °C reduced the energy required for heating and vaporisation by 40.5%. In addition, an average solar radiation of 85.15 W/m² was reported to have increased the SW temperature by 109%. The effect of ambient temperature on the desalting process was such that for every 5 °C increase in ambient temperature, the SW temperature increased by 5.49 °C, reducing the thermal energy required for heating and evaporation. The study also noted that desalination is limited when the thermal energy input rate is below 500 W/m². The highest distillate yield was 4.55 kg/h.

Zhu et al. (2022) reported that the distillate production efficiency of the solar still with and without heat recovery was the highest at 31.7% and 37.0%, respectively. The distillate yield of the solar still with heat recovery was up to 44.3% higher than the solar still without heat recovery. The SW evaporation efficiency was reported to be highest at 57.8% and 49.5% for solar stills with and without heat recovery and SW preheating, respectively. Fallahzadeh et al. (2020) studied solar stills with and without preheating air injected into the still. The system was equipped with a heat recovery mechanism in which uncondensed vapour was sent to the evaporation section, where the condensed vapour released its latent heat to the SW in the tank. In addition, without air preheating, the solar still productivity was 10% and 9% lower when powered at 585 W/m² and 210 W/m², respectively. The preheating of the air increased the humidity and facilitated the evaporation of SW. However, the increased surface area of the distiller reduced the instantaneous efficiency.

Özcan and Deniz (2023) reported that the improved solar still with heat recovery achieved thermal efficiency of 40.34%, outperforming the conventional solar still (CSS) with 35.55% thermal efficiency. In addition, the modified solar still increased productivity by 13.44%, surpassing that of CSS.

Sharshir et al. (2023) reported that SW preheating is not a mere process but allows for accelerated evaporation, prolonging the evaporation process even at low

insolation and ambient air temperatures and minimising heat loss from the SW. A solar still developed by Rajaseenivsan et al. (2016) maintained preheated SW at 10 °C higher than the CSS later during off-sunshine hours. This indicated that the evaporation process was prolonged in the solar still with preheated SW. Moreover, the preheated SW in the preheater was inversely proportional to its depth due to the increased thermal inertia of the water mass. However, the larger body of water was advantageous, because the stored thermal energy was released during off-sunshine periods, and desalination continued. In a study by Abd Elbar and Hassan (2020), SW preheating was performed by a solar panel (SP), and the preheated SW remained 5 °C higher than the CSS, resulting in enhanced evaporation rate and productivity. However, it was further reported that increasing the feedwater flow reduced the preheating temperature at the SP outlet from a maximum of 41.4–39.1 °C. In contrast, the SP was cooled by increasing the feedwater flow rate, which enhanced its thermal energy efficiency and increased the temperature across the SW in the pool up to 68.3 °C. Thus, balancing the contributing factors (e.g., heat input rate, SW preheating, wind cooling effects, etc.) could result in optimal heat recycling and enhanced distillate output.

Furthermore, heat recovery reduces heat losses as heat recovery uses a significant portion of the latent heat of condensation to raise the feedwater temperature without additional heat energy storage (Aboabboud et al., 1997; Chen et al., 2023). Several other studies have implemented SW preheating and heat recovery to improve productivity and thermal efficiency by altering SW flow composition, geometry, condensation and vaporisation effects, and a reduction in cost per litre (CPL) has been reported (Kaushal et al., 2017; Liu et al., 2014; Schwarzer et al., 2009).

The literature reviewed and discussed above indicates that researchers have made various attempts to improve the performance of solar thermal desalination systems through heat recovery and SW preheating methods. However, none of the above studies identified the flow configurations proposed in the current study.

Therefore, this study aims to report the heat recycling capability of a vapour-based multistage solar still with stacked stages (MSS–SS) with its distinct configurations. This study identified various recent published research on the shortcomings of solar stills in recovering and reusing generated thermal energy. The current paper contributes to methods and approaches for recovering thermal energy in desalination plants. This work complements recently published work on the same desalination plant (Mkhize & Msomi, 2022, 2023). Three representative days were chosen to analyse and discuss the SW

preheating, heat recovery, condensing tower, evacuated tube solar collectors (ETSCs), and overall system thermal efficiencies.

Description of the system

A detailed description of the condensing tower shown in Fig. 1 can be found elsewhere (Mkhize and Msomi, 2022). The work will focus on heat recovery and SW preheating components. The thermal energy the evacuated tube solar collectors (ETSCs) provide passes through the evaporator and vapour-make-up tubes indicated by the “vapour flow” arrows and finally injected into the five-stacked stages. A 15 mm outside diameter (OD) tube (not shown) carried raw SW supplied from the external SW tank. Heat transfer occurred between this tube’s relatively cold raw SW, indicated by the “light green” arrows, and the rising vapour. Multi-effect SW preheating and heat recovery occurred at each stage, while the SW flowed down through the 15 mm tube under the gravitational influence. The raw SW was collected in a preheated state in the secondary SW tank with a capacity of 2.7 kg.

The temperature in the secondary SW tank (dark green arrows) indicated the cumulative SW preheating of the entire unit. The preheated SW was transferred from the secondary SW tank to the vaporiser for further heating and vaporisation. Each stage produced its distillate and

sent it to the distillate tank, as indicated by the ‘black arrows’. The SW was heated in a series of connected ETSCs and evaporated in the evaporator. The heated SW in the evaporator did not rise to the Stages but was recirculated in the open loop circuit of the evaporator and ETSCs, as indicated by the ‘red arrows’. In addition, the outer shell of the condensing tower was insulated with a 25 mm thick polystyrene material at a given solar intensity. However, due to the low thermal inertia of the water body, the insulation was removed to prevent overheating of the system when the sun was intense. The body of the condensing tower was made from a 0.9 mm thick aluminium plate that provided a condensation surface for the vapour.

Experimental procedure

The experimental tests were conducted at Cape Peninsula University of Technology (CPUT), Bellville campus, Cape Town, South Africa. During the experimental testing, the system continuously recorded data for solar irradiance, wind speed, ambient air temperature and SW temperature 24 h per day. BTM-4208SD 12 channel temperature data logger recorded temperature data. Details of the experimental procedure, equipment procedure, equipment used, precision, and error data have been provided elsewhere (Mkhize & Msomi, 2022, 2023).

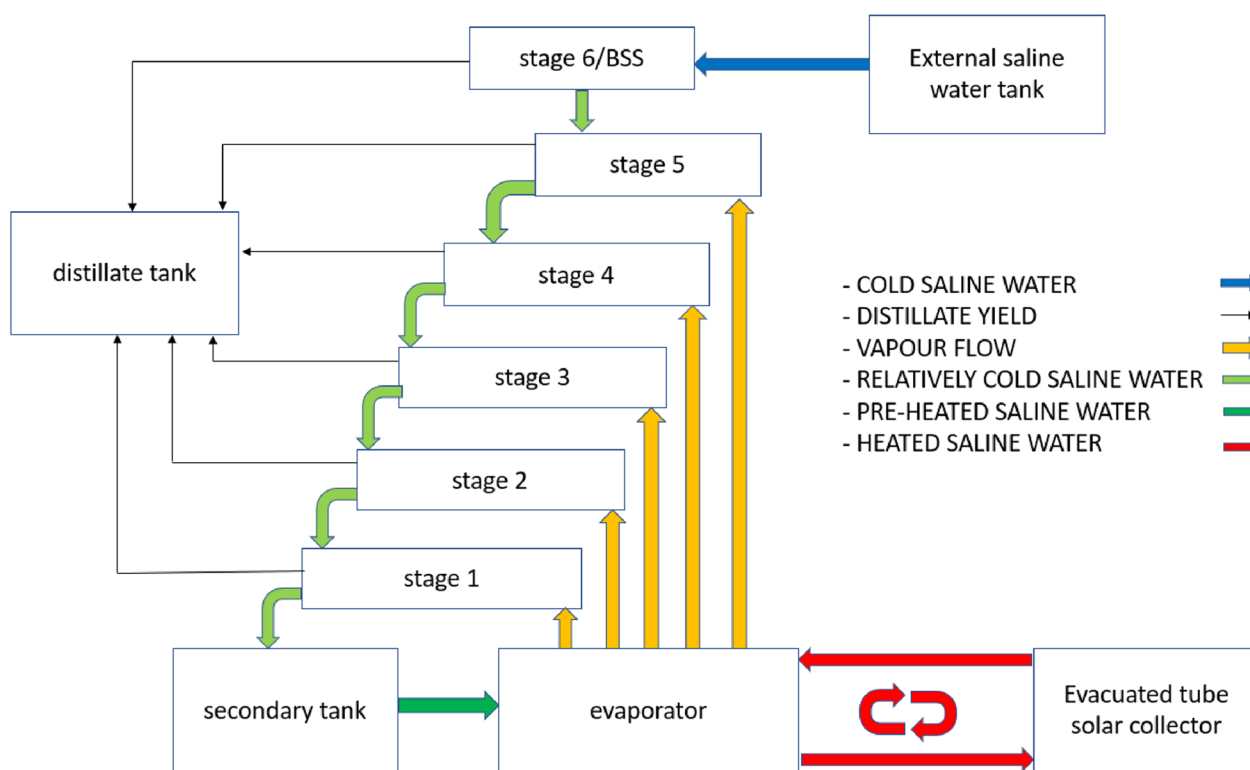


Fig. 1 Schematic diagram of the desalination unit

Energy balance of the system

- The amount of SW evaporated in the evaporator corresponds to the condensed water fraction as distillate in the stages.
- Heat loss from the vapour to the walls of the vapour make-up tubes is negligible.
- Preheating by the SW in the basin solar still (BSS), also called stage 6 (refer to Fig. 1), is considered negligible in the numerical analysis.
- Heat loss from the zig-zagged SW tube is negligible.
- The distillate temperature leaving the stage is the same as that of the stage.
- The vapour temperature in the stage is the same as the evaporator temperature.
- The energy balance is formed when the system is stable and operates properly under steady conditions.
- The vapour transfer through the vapour transfer tubes is negligible, and the vapour is considered to condense completely in a stage.
- No condensable gases and their effects are ignored.

Chen et al. (2017) reported that the hourly solar irradiance and the collector efficiency can express the thermal energy collected by the ETSC. That is

$$\dot{Q}_{ETSC} = I_{\beta} \times \eta \quad \left(\text{W/m}^2 \right) \tag{1}$$

$$\eta = 0.803 - 2.01 \left(\frac{T_m - T_a}{I_{\beta}} \right) - 0.0034 \left(\frac{(T_m - T_a)^2}{I_{\beta}} \right) \times 100\% \tag{2}$$

T_m , is the mean temperature of SW in the ETSC (K), T_a , is the ambient temperature (K) and I , is the collected solar irradiance (W/m^2).

Considering the SW in the evaporator with negligible heat losses:

$$\dot{Q}_{ETSC} = \dot{Q}_{evap} = \dot{m}_{sw} \cdot cp \cdot \frac{dT}{dt} + (\dot{m}_e hf_g)_{evap}. \tag{3}$$

Heat and mass transfer in the condensing tower

In Eq. 3, when moving from the left-hand side to the right-hand side, the distribution of total energy absorbed by the ETSCs, the energy utilised for heating the SW, and the energy responsible for vapourising the water.

Given that the SW was recirculated in the evaporator and only the vapour reached stages 1–5, the total energy reaching these stages can be expressed as $(\dot{m}_e hf_g)_{evap}$.

That is

$$(\dot{m}_e hf_g)_{evap} = \sum_{i=1}^5 \dot{m}_e hf_g \tag{4}$$

$$(\dot{m}_e hf_g)_{evap} = \dot{m}_{e,1} hf_{g1} + \dot{m}_{e,2} hf_{g2} + \dot{m}_{e,3} hf_{g3} + \dot{m}_{e,4} hf_{g4} + \dot{m}_{e,5} hf_{g5} \tag{5}$$

where hf_{g1} , hf_{g2} , hf_{g3} , hf_{g4} , and hf_{g5} , are the evaporative thermal energy terms in kJ/kg and $\dot{m}_{e,1}$, $\dot{m}_{e,2}$, $\dot{m}_{e,3}$, $\dot{m}_{e,4}$, and $\dot{m}_{e,5}$ are the mass flow rates of the vapour in kg/s reaching the stages, respectively.

Figure 2 shows schematically, the two exploded stages of a vapour-based MSS–SS and their thermal energy flow patterns. The term, $\dot{m}_{sw} \cdot cp \cdot T$, is the preheated SW passing through the stage from the BSS, but this term can only be determined accurately for stage 5. From 1st to 4th stage, the SW is preheated, and the heat is recovered after each stage. Therefore, the effect of the vapour from the vapour make-up tubes must be considered:

$$\dot{Q}_{loss} = \sum_{i=1}^5 \dot{q}_{losses}$$

Therefore, the thermal energy exchange in stage 1 is

$$\dot{m}_{e,1} hf_{g1} = \dot{m}_{sw,1} \cdot cp_{sw} \cdot \frac{dT}{dt} + \dot{m}_{dist,1} \cdot cp_{dist,1} \cdot T_{s1} + \dot{Q}_{loss,1}. \tag{6}$$

The terms, $\dot{m}_{sw,1} \cdot cp_{sw,1} \cdot \frac{dT}{dt}$, $\dot{m}_{dist,1} \cdot cp_{dist,1} \cdot T_{s1}$ and $\dot{Q}_{loss,1}$ refers to the real-time thermal energy absorbed by the zig-zagged SW tube in the first stage, the thermal energy carried by the distillate as it exits the stage, and the thermal energy dissipated through the stage’s walls.

Given the assumption that the quantity of evaporated seawater equals the quantity of condensed distillate, that is $\dot{m}_{e,1} = \dot{m}_{dist,1} = \dot{m}_1$.

Therefore, Eq. 6 becomes:

$$\dot{m}_1 (hf_{g1} - cp_{dist,1} \cdot T_{s1}) = \dot{m}_{sw,1} \cdot cp_{sw,1} \cdot \frac{dT}{dt} + \dot{Q}_{loss,1}. \tag{7}$$

For stages 2, 3, 4 and 5, the equations are as follows, respectively:

$$\dot{m}_2 (hf_{g1} - cp_{dist,2} \cdot T_{s2}) = \dot{m}_{sw,2} \cdot cp_{sw,2} \cdot \frac{dT}{dt} + \dot{Q}_{loss,2} \tag{8}$$

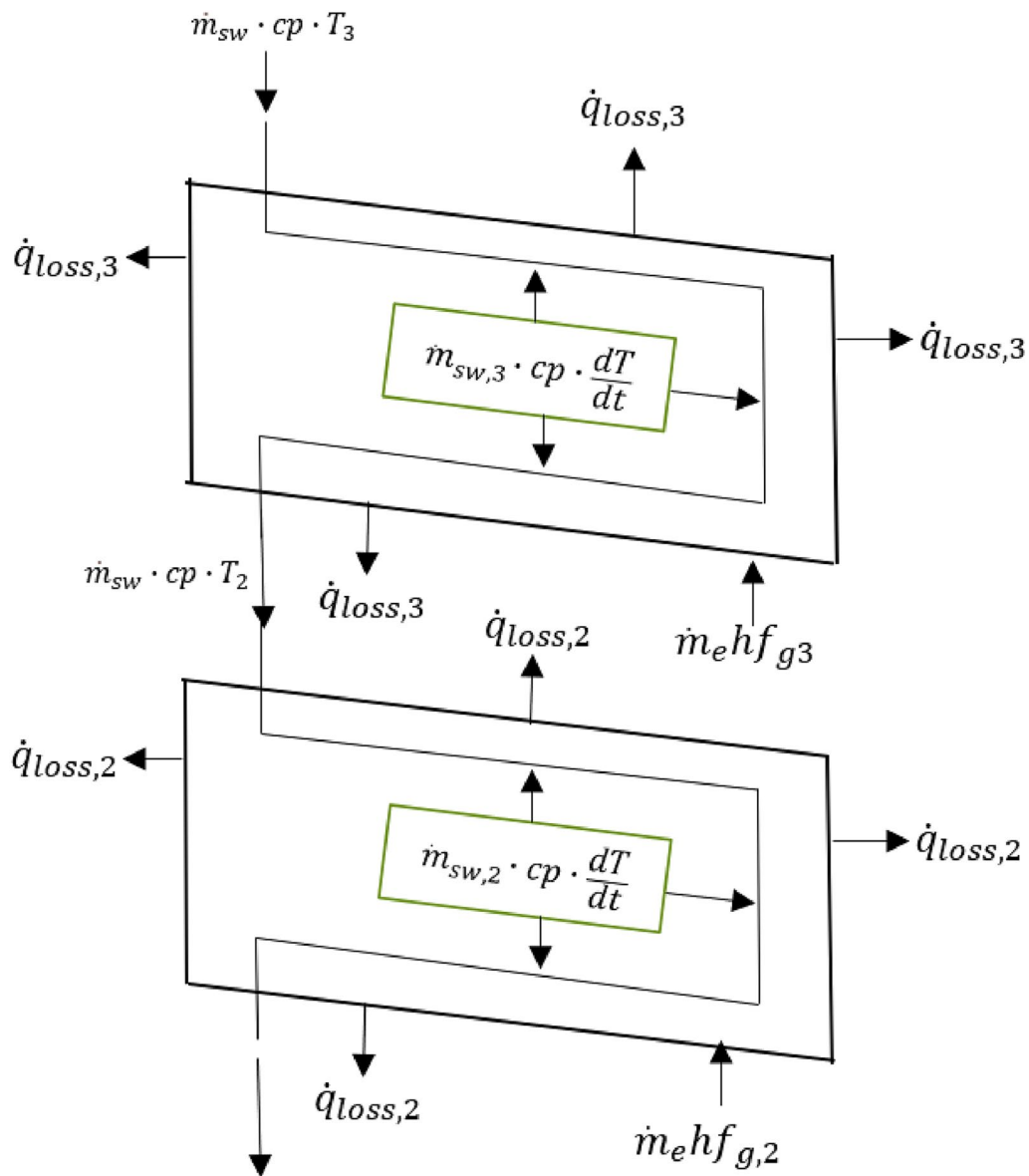


Fig. 2 Thermal energy flow pattern

$$\dot{m}_3(hf_{g3} - cp_{dist,3} \cdot T_{s3}) = \dot{m}_{sw,3} \cdot cp_{sw,3} \cdot \frac{dT}{dt} + \dot{Q}_{loss,3} \tag{9}$$

$$\dot{m}_4(hf_{g4} - cp_{dist,4} \cdot T_{s4}) = \dot{m}_{sw,4} \cdot cp_{sw,4} \cdot \frac{dT}{dt} + \dot{Q}_{loss,4} \tag{10}$$

$$\dot{m}_5(hf_{g5} - cp_{dist,5} \cdot T_{s5}) = \dot{m}_{sw,5} \cdot cp_{sw,5} \cdot \frac{dT}{dt} + \dot{Q}_{loss,5} \tag{11}$$

where T_s is the condensing surface temperature ($^{\circ}\text{C}$), cp_{dist} specific heat capacity of the distillate ($\text{kJ}/\text{kg } ^{\circ}\text{C}$), cp_{sw} specific heat capacity of SW ($\text{kJ}/\text{kg K}$). Heat losses in each stage is:

Specific heat capacity and the density of SW were estimated from (Koffi et al., 2008):

$$C_p = 4226 - 3.244T + 0.0575T^2 - 0.0002656T^3 \tag{12}$$

$$\rho = 1001 - 0.08832T + 0.003417T^2 \quad (\text{kg/m}^3). \tag{13}$$

Furthermore, the following equations were used for estimating the evaporative energy (kJ/kg) both below and above SW temperatures of 70 °C (Mbadinga, 2015).

$$hfg_{\text{evap}} = 3.1615 \times 10^6 \times [1 - (7.616 \times 10^{-4} T_{\text{sw}})] \quad T > 70^\circ\text{C} \tag{14}$$

$$hfg_{\text{evap}} = 2.4935 \times 10^6 \left[\left(1 - 9.4779 \times 10^{-4} T_{\text{sw}} \right) + \left(1.3132 \times 10^{-7} T_{\text{sw}}^2 \right) - \left(4.7979 \times 10^{-9} T_{\text{sw}}^3 \right) \right] \quad T < 70^\circ\text{C} \tag{15}$$

The thermal efficiency of the condensing tower is

$$\eta = \frac{\text{Useful energy}}{\text{Energy supplied by the ETSC}}$$

$$\eta = \frac{(\dot{m}_e hfg)_{\text{evap}}}{\dot{Q}_{\text{ETSC}}} \times 100\%. \tag{16}$$

The overall efficiency of the system is

$$\eta = \frac{(\dot{m}_e hfg)_{\text{evap}}}{\text{Energy received by the ETSC or energy reaching the aperture area of the ETSC}}$$

$$\eta = \frac{(\dot{m}_e hfg)_{\text{evap}}}{I(t)} \times 100\%. \tag{17}$$

The thermal energy collected by the ETSCs (Maleki et al., 2017; Diez et al., 2021).

The total solar radiation on a horizontal surface is given by the combination of beam and diffuse radiation components:

$$I_H = I_b + I_d \quad (\text{W/m}^2). \tag{18}$$

The sky's hourly clearness index:

$$M_t = \frac{I_H}{I_o}. \tag{19}$$

In addition, the extra-terrestrial radiation, I_o

$$I_o = \left(\frac{12 \times 60}{\pi} \right) I_{\text{sc}} E_o [(\omega_{ii} - \omega_i) \sin\varphi \sin\delta + \cos\varphi \cos\delta (\sin\omega_{ii} - \sin\omega_i)] \quad \left(\frac{\text{MJ}}{\text{m}^2 \text{ h}} \right). \tag{20}$$

The solar constant is $I_{\text{sc}} = 1367 \text{ W/m}^2$ and the eccentricity correction factor E_o is

$$E_o = 1 + 0.033 \cos \left(\frac{2\pi n}{365} \right). \tag{21}$$

The duration hour angle, ω_1 and ω_2 , where t_1 is the time duration:

$$\omega_i = \omega - \left[\frac{(\pi \times t_d)}{24} \right] \tag{22}$$

$$\omega_{ii} = \omega + \left[\frac{(\pi \times t_d)}{24} \right]. \tag{23}$$

The parameter, B with n representing the day in a year

$$B = \frac{2\pi(n - 81)}{365}. \tag{24}$$

Then, the equation of time is

$$ET = 9.87 \sin 2B - 7.53 \cos B - 1.5 \sin B. \tag{25}$$

In addition, the solar time:

$$ST = 4(L_s - L_{\text{loc}}) + ET + LT. \tag{26}$$

The seasonal correlation factor for solar time, S_c .

$$S_c = 0.1645 \sin 2B - 0.1255 \cos B - 0.025 \sin B. \tag{27}$$

The hour angle, where t is the standard time at the mid-point of the period:

$$\omega = \frac{\pi}{12} [(t + 0.06667(L_s - L_L) + S_c) - 12]. \tag{28}$$

Then, the declination angle, δ

$$\delta = 0.409 \sin \left[\left(\frac{2\pi n}{365} \right) - 1.39 \right]. \tag{29}$$

The hourly diffuse fraction (k_d) on the horizontal surface:

$$M_t \leq 0.21 \quad k_d = 0.995 - 0.081 M_t \tag{30}$$

$$0.21 < M_t \leq 0.76, \quad k_d = 0.724 + 2.738 M_t - 8.32 M_t^2 + 4.967 M_t^3 \tag{31}$$

$$M_t > 0.76 \quad k_d = 0.18 \tag{32}$$

$$k_d = \frac{I_d}{I_H} \tag{33}$$

The total hourly radiation on an inclined surface is

$$I_\beta = I_{b\beta} + I_{d\beta} + I_r \quad (\text{W/m}^2). \tag{34}$$

Hays anisotropic index

$$f_{\text{Hay}} = \frac{I_b}{I_o} = \frac{I_H - I_d}{I_o} \tag{35}$$

The diffuse component on an inclined surface:

$$I_{d\beta} = I_d \left[f_{\text{Hay}} \left(\frac{\cos\theta}{\cos\theta_z} \right) + \left(\frac{1 + \cos\beta}{2} \right) (1 - f_{\text{Hay}}) \right] \quad (\text{W/m}^2). \tag{36}$$

In addition, the beam component is

$$I_{b\beta} = I_b R_b \quad (\text{W/m}^2). \tag{37}$$

With the tilt factor given by

$$R_b = \frac{\cos\theta}{\cos\theta_z} \tag{38}$$

The incidence and zenith angles are

$$\cos\theta_z = \cos\delta\cos\varphi\cos\omega + \sin\varphi\sin\delta \tag{39}$$

$$\cos\theta = \cos(\varphi + \beta)\cos\delta\cos\omega + \sin(\varphi + \beta)\sin\delta. \tag{40}$$

In addition, the reflected radiation on the ground is as follows:

$$I_r = I_H \rho_g \left(\frac{1 - \cos\beta}{2} \right) \quad (\text{W/m}^2). \tag{41}$$

Substituting Eqs. 36, 37 and 41 into Eq. 34, one obtains the total hourly radiation on an inclined surface which can be multiplied by the number of hours to arrive at the total energy collected a day.

Results and discussion

Solar radiation on an inclined surface

This section discusses three specific dates. November 12, 2020, was chosen due to its highest SW preheating performance; January 13, 2021, was selected for its overall highest distillate production; and June 26, 2021, stood out as one of the lowest in terms of SW preheating, heat recovery, and distillate yield from the MSS–SS. In addition, the distillate yield from the stacked stages (excluding the BSS) was precisely the same on November 12, 2020, and January 13, 2021. Solar radiation plays a crucial role in the operation of the solar still (Fallahzadeh et al., 2020). To make it easier to reference, the average solar

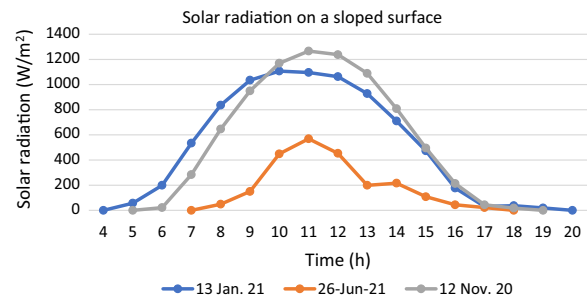


Fig. 3 Condensing tower thermal efficiency

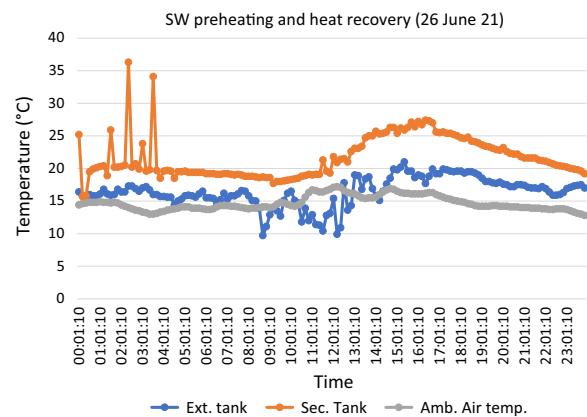


Fig. 4 External tank and secondary SW

radiation intensities have been categorised into three groups: 0–199 W/m² for low, 200–399 W/m² for moderate, and 400–600 W/m² for high ranges.

Furthermore, the total daily thermal energy collected by northward-facing ETSCs with a slope of 56° from the horizontal was estimated at 30,821.04, 30,780.0, and 8427.6 kJ/m² for November 12, 2020, January 13, 2021, and June 26, 2021, respectively. The total daily thermal energy was obtained by utilising Eqs. 1, 2 and 18–41 (Diez et al., 2021; Maleki et al., 2017). Figure 3 illustrates the daily solar radiation on these two-sloped ETSCs, with the winter day (June 26, 2021) receiving significantly lower intensity. It is also evident from the figure that November 12, 2020, experienced the highest peak in solar radiation, resulting in increased thermal energy collection.

SW preheating and heat recovery

The temperature difference between the external SW tank (ext. tank) and the secondary tank (sec. tank) served as an indicator for assessing the degree of SW preheating and heat recovery. A greater temperature differential indicated an enhancement in either heat recovery and SW preheating or solely SW preheating, particularly in uninsulated condensing tower cases. Notably,

experimental observations revealed that removing insulation material impacted desalination as the condensing tower body was exposed to the environment. On the 26th of June 2021, the average daily solar radiation, wind velocity and ambient air temperature were recorded as 209.81 W/m², 2.66 m/s and 15.66 °C, respectively, measured at the beginning of the day. Figure 4 illustrates the temperatures of the secondary SW tank, external tank, and the ambient air on this specific day.

The test rig yielded 510 ml of distilled water, with 170 ml produced by the BSS and 340 ml by the five-stacked stages. This resulted from low solar insolation, and these days were most common during winter and occasionally occurred in the spring and autumn, characterised by limited solar radiation and cooler surroundings (Mkhize & Msomi, 2023). In addition, there was an early morning temperature spike to a maximum of 36.3 °C due to residual preheated SW flowing into the secondary tank from the previous day. Subsequently, the secondary SW temperature gradually decreased by 2.7 °C before the heating phase, which commenced shortly after sunrise. This decline was attributed to the relatively small temperature difference between the SW in the secondary tank and the ambient air temperature.

The secondary SW tank reached its peak temperature of 27.4 °C around 4 PM, which was 9.7 °C higher than the temperature of the external tank, indicating the extent of SW preheating. The average temperatures of the external and secondary tanks, measured at the beginning of the day, were 16.03 °C and 22.38 °C, respectively. These prevailing conditions formed the basis for unproductive MSS–SS. The experiments revealed a marginal average temperature difference of a mere 6.35 °C between the secondary and external tanks, which could have resulted from two potential issues. First, the low ambient conditions may have increased heat loss through convective and radiative heat transfer to the surroundings. Second, it might have been due to insufficient vaporisation energy injected into the stacked stages, as defined by Eq. 5. Overall, the MSS–SS experienced minimal productivity, heat recovery and SW preheating under these conditions, suggesting that it was unsuitable to operate efficiently.

The slight temperature difference resulting from the latter factor led to reduced overall and condensing tower thermal efficiencies, as described by Eqs. 16 and 17. The overall daily thermal efficiency was estimated at 5.89%, signifying increased heat wastage to the environment despite the insulation material on the condensing tower's body. In addition, as mentioned elsewhere, the vapour make-up tubes served as a thermal boundary layer, especially in the morning when the system components were cooler and solar intensity was low. The heat generated by the ETSCs was used to heat and establish thermal

equilibrium in these vertically oriented tubes. Until the equilibrium was achieved, vapour delivery into the stages failed. Thus, the experimental tests revealed a strong correlation between the thermal energy input, SW preheating and distillate output.

On the 13th of January 2021, the average solar radiation, wind speed and ambient air temperature were measured at 585 W/m², 3.12 m/s and 29.34 °C, respectively. An increase of 64.14%, 46.63% and 14.74% in the three meteorological conditions, respectively, compared to the previous day. With these conditions, the test rig produced the highest distillate yield of 7790 ml, with 6730 ml from the five stacked stages only and 1060 ml by the BSS (Mkhize & Msomi, 2023). Furthermore, the SW temperature in the secondary tank dropped by 10 °C from midnight to its lowest point of 31 °C around 6 AM before the heating phase commenced. This drop was more significant than the 2.7 °C observed on the 26th of June 2020, indicating greater heat transfer to the surroundings due to a larger temperature difference with the ambient air. Moreover, in Fig. 5, a more noticeable temperature difference was evident due to the increased product value of the evaporative term and vapour flow rate into the stages, as defined by Eq. 5. The SW temperature in the external tank was higher than on the previous day due to the elevated ambient air temperature.

The experimental tests demonstrated that the desalination process was closely correlated with the prevailing ambient conditions, as reported in the literature. Despite the challenges posed by the thermal damage conditions, which led to the removal of the insulation material from the condensing tower's body, the SW was preheated to 66.8 °C. However, removing the insulation reduced heat recovery, since the condensing tower body was exposed to the environment. Furthermore, due to the high collector-to-basin area (CBA) ratio and the low thermal inertia of the water mass, SW preheating reached the maximum of 66.8 °C despite increased heat loss to the environment due to insulation material removal.

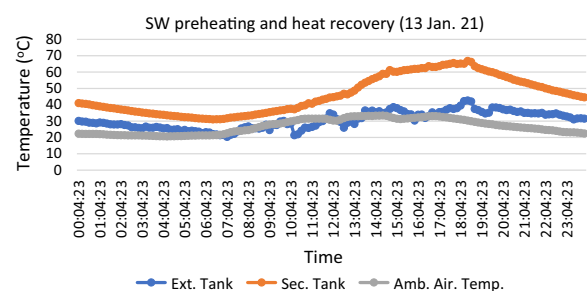


Fig. 5 External tank and secondary SW

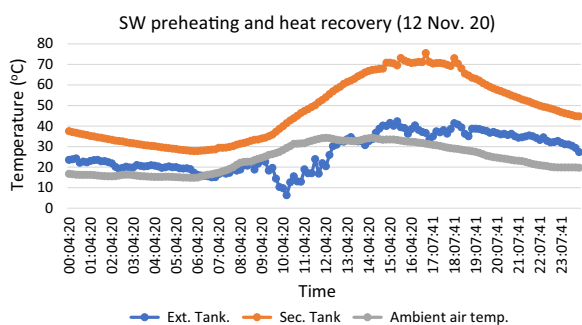


Fig. 6 External tank and secondary SW

A maximum temperature difference of 24.2 °C between the secondary and external tanks was achieved at the peak temperature after 6 PM. This temperature difference was 17.2 °C higher than the same value on the 26th of June 2021. Based on the substantial average velocity increase of 46.63%, it was concluded that the wind velocity was responsible for enhancing the desalination in the test rig. The ambient air temperature effects were minimal. Furthermore, the delayed peak temperature in the secondary tank resulted from a larger volume of SW (Mkhize & Msomi, 2022). This pattern was consistently observed throughout the experimental tests. In addition, it was observed that reusing heated SW improved the evaporation process, thereby requiring less thermal energy to heat and vaporise SW in the evaporator. Consequently, the overall daily thermal efficiency increased to 28.31%, which can be attributed to solar radiation and the wind velocity effects. However, it could have been even higher if thermal insulation had remained on the condensing tower’s body, were it not for the thermal damage conditions.

On November 12, 2020, as depicted in Fig. 6, the condensing tower underwent testing with the same operational parameters as those on January 13, 2021. The experimental setup yielded a distillate volume of 7500 ml during this test. Of this total, 6730 ml was produced by the five stacked stages, while the BSS produced 770 ml. Consequently, the five-stacked stages (excluding the BSS) produced equivalent distillate on both days, with the BSS accounting for the variation. The average solar radiation, wind speed and ambient air temperature were 581.8 W/m², 1.54 m/s and 28.0 °C, respectively. Under these specific meteorological conditions, there was an average decline of 0.55%, 4.55%, and 50.64% in the meteorological conditions. Comparing November 12, 2020, with June 26, 2021, the averaged solar radiation and ambient air temperature increased by 63.94% and 44.1%, respectively, while the velocity declined by 42.1%. Furthermore, the experiments

indicated increased heat losses on January 13, 2021, as the same amount of distillate was produced with less heat input for the stacked stages (excluding the BSS).

Furthermore, SW preheating reached a maximum temperature of 75.5 °C, confirming the surrounding conditions’ significant impact on desalination, especially since the condensing tower lacked insulation. A larger temperature differential of 38.9 °C between the secondary and external tanks reduced thermal energy requirements for heating and vaporisation in the evaporator.

Due to the enhanced preheating and heat recovery observed on November 12, 2020, the overall thermal efficiency increased to 33.83%. This marked a 5.52% rise compared to the previous day. Moreover, it is evident that by minimising heat losses to the surroundings through applying insulation material under various operating conditions, SW preheating, distillate output and heat recovery can be improved, ultimately boosting thermal efficiency. Hence, these configurations that maximise SW preheating and heat recovery demonstrated significant potential for conserving and enhancing the thermal efficiency of the desalination system.

Effects of wind velocity

The wind velocity profiles presented in Fig. 7 for the three specific days are the basis for establishing a connection between SW preheating and the cooling influence of wind on the condensing tower’s structure. On the 13th of January 2021, during the daytime desalination phase, there was a higher wind velocity, which led to cooling effects on the condensing tower. This phenomenon was not observed on the 12th of November 2020. The impact of wind velocity on the desalination process can be linked to the cooling effect it has on the condensing tower’s surface, which aids in enhancing the condensation process. Even in high ambient air temperature and solar radiation, a high wind velocity maintained a significant temperature

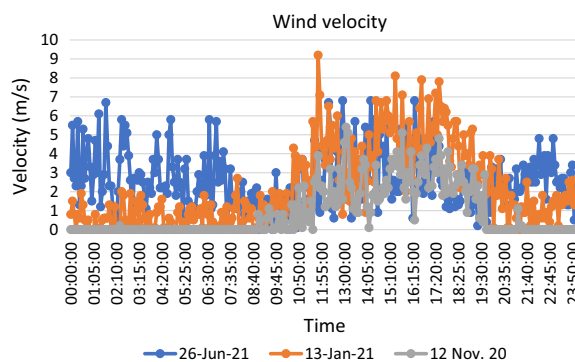


Fig. 7 External tank and secondary SW

difference between the evaporative and condensing surfaces (Mkhize & Msomi, 2023). However, the drawback of high wind velocity was that it limited the SW preheating and made heat recovery ineffective. Consequently, the level of SW preheating on the 13th of January 2021 was lower than on the 12th of November 2020.

On the 12th of November 2020, the average wind speed was 50.64% lower than the 3.12 m/s observed on the 13th of January 2021, reducing cooling effects on the condensing tower. This leads to the conclusion that low wind velocities were advantageous for SW preheating and heat recovery processes (when insulation was applied) but were less favourable for condensation. As a result, the overall distillate yield was higher on the 13th of January 2021 despite the higher average solar radiation. Furthermore, compared to the 26th of June 2021, it was concluded that unlike on the 13th of January 2021, where the average velocity increased by 46.63%, a decline of 42.1% on the 12th of November 2020 negatively affected the overall distillate output. Thus, there was a strong correlation between the enhanced distillate output and wind velocity. However, it is important to note the influence of various factors in addition to the wind velocity effects as it did not act in isolation. For instance, on the 26th of June 2021, with low solar radiation and ambient air temperature, high wind velocities proved detrimental to the desalination process and overall thermal efficiency. This indicates that a combination of factors, including wind velocity, ambient air temperature, solar radiation and more, collectively determine the extent of the desalination process, SW preheating and heat recovery when considering an insulated condensing tower. Hence, it is important to note that the operating conditions in the field test are not universally fixed and inflexible.

Effects of ambient air temperature

Based on Fig. 8 and the average data, the ambient air temperature on November 12, 2020, was 1.34 °C lower

than the 29.43 °C recorded on January 13, 2021. This temperature difference was advantageous for condensation but not favourable for SW preheating and heat recovery. However, due to the low wind velocities, the secondary tank SW achieved its highest temperature of 75.5 °C. This suggests that the interplay of all factors comes into play and occurs dynamically in most cases. This was supported by the fact that despite reaching maximum temperatures of 75.5 °C and 66.8 °C on the two respective days, the secondary SW tank temperature on November 12, 2020, was only 0.2 °C higher than that on January 13, 2021, by the end of the day, indicating increased heat transfer to the environment.

The lower average ambient air temperature on November 12, 2020, in the early morning and later in the day, increased heat losses to the surroundings, leading to a rapid decline in SW temperature throughout the system. Figure 8 shows that the ambient temperature on November 12, 2020, was initially higher, reaching a maximum of 34.3 °C up until 4 PM, but was surpassed after that time. This implies that the ambient air temperature, linked with accompanying factors, positively impacted SW preheating for most of the day on November 12, 2020, compared to January 13, 2021, despite a slightly lower average temperature of 28.0 °C.

Regarding the distillate output, an increase in ambient air temperature stifled the overall productivity of the test rig. It can be observed that there was a 14.74% and 44.1% increase in ambient air temperature between the 26th of June 2021 and 13th of January 2021 and the 13th of January 2021 and 12th of November 2020, respectively. In the former increase (14.74%), the distillate was the highest, while the latter (44.1%), the overall distillate was lower. Therefore, it can be similarly concluded that the higher ambient air temperature negatively affects the overall distillate output.

The observations further concluded that, while the increase in ambient air temperature negatively affected

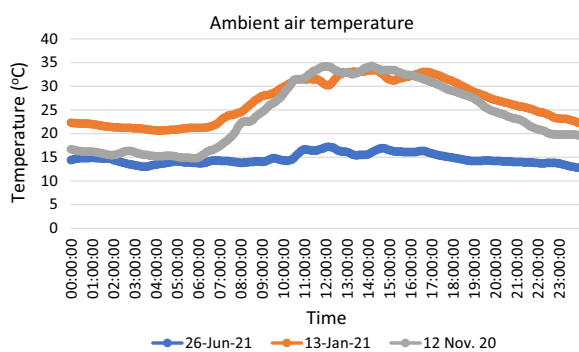


Fig. 8 External tank and secondary SW

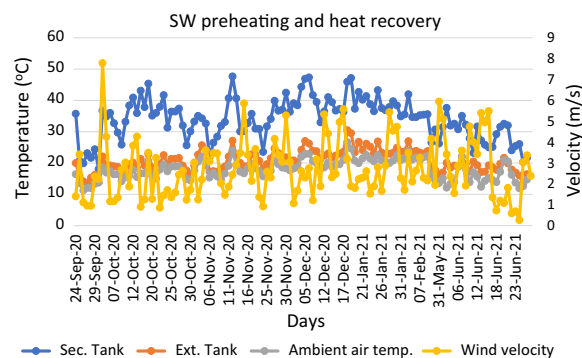


Fig. 9 External tank and secondary SW

the distillate, A strong correlation was observed between increasing ambient air temperature and the enhancement of the overall thermal efficiency. There was a much better thermal energy conservation with higher ambient air temperature.

Seasonal effects of wind velocity and ambient air temperature

Figure 9 illustrates the relationship among four key parameters: ambient air temperature, secondary SW tank temperature, external SW tank temperature and wind velocity throughout the experimental period. The highest SW preheating coincides with the highest ambient air temperatures in late spring, elevating the external SW tank temperature. In addition, the secondary tank SW maintains higher temperatures during summer, indicating that desalination is most effective. As summer approached, the gradual increase in ambient air temperature facilitated heating and evaporating at high rates with reduced energy input. This was evident from the 34.3 °C temperature reached on November 12, 2020, and the higher overall thermal efficiency achieved under similar operating conditions. Consequently, the desalination process experienced a decline as winter approached and during the winter season.

Figure 9 portrays the correlation between the ambient air temperature, secondary SW tank temperature, external SW tank temperature and wind velocity for the entire experimental test duration. The experiments revealed higher ambient air temperatures were generally associated with enhanced secondary tank SW preheating. However, in late February 2021, there was a sharp drop in ambient air and external tank temperature, followed by a decline in secondary SW tank temperature. This necessitated increased thermal energy injection into the test rig to initiate and maintain desalination. Nevertheless, an overall increasing trend was noticeable from early spring to late summer. This implied that distillate can be produced even on cooler days in autumn, summer, and spring, with the peak occurring in mid-summer. The wind was most prevalent in the late spring, summer, and winter seasons. The experimental test determined a strong correlation between higher wind velocities during the late spring and summer seasons and the benefits of the overall desalination process by sufficiently cooling the condensing tower. However, during winter, coupled with much cooler days, higher wind velocities reduced overall thermal efficiency by increasing heat losses from the condensing tower’s walls. To achieve higher productivity, the condensation rate needed to be improved.

For enhanced SW preheating and heat recovery, insulating the condensing tower effectively from its surroundings was crucial to ensuring sufficient SW with higher thermal inertia of water mass to recover and store heat. This would, in turn, lead to improved overall and condensing tower thermal efficiency. However, this approach could be contradictory, because exposure to wind velocity facilitates cooling, enhances condensation, and increases heat losses. A well-insulated condensing tower enables better SW preheating and heat recovery but may reduce the condensation rate and, subsequently, the distillate yield. Both approaches have the potential to impact desalination efficiencies. Therefore, it is prudent to balance these factors to maximise distillate production while accepting an acceptable compromise regarding thermal efficiency.

Overall, condensing tower and ETSCs thermal efficiencies

Based on the theoretical model developed, this section delves into the performance of the condensing tower on the selected days.

The overall daily thermal efficiencies were estimated at 5.89%, 28.31% and 33.83% for June 26, 2021, January 13, 2021, and November 12, 2020, respectively. Notably, the highest thermal efficiency achieved for the condensing tower throughout the experimental tests was 33.83%. This was slightly higher than some of the desalination systems found in the literature (Zhu et al., 2022). Furthermore, Fig. 10 illustrates the hourly thermal efficiency of the condensing tower. These thermal efficiency estimates assumed that hourly distillate production remained constant. At the start of the desalination process in the morning, despite the thermal boundary in the vapour make-up tubes, the figure demonstrates a higher condensing tower thermal efficiency of approximately 34.1% for June 26, 2021, and 57.52% for November 12, 2020. However, there was a sharp decline in the subsequent hours, with hourly

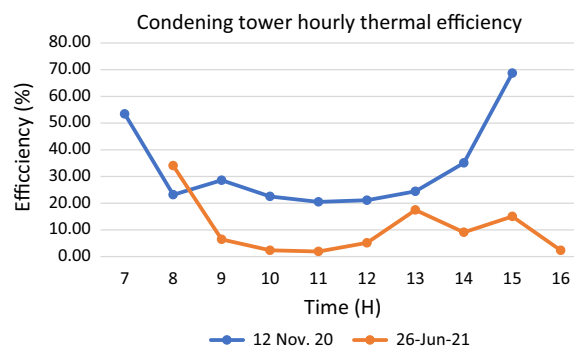


Fig. 10 Condensing tower thermal efficiency

thermal efficiencies dropping as low as 1.97% and 19.6% for the respective days. Such reduced efficiency was associated with increased heat losses to the surroundings due to the low thermal inertia of the water mass and the rising solar intensity approaching noon.

During heating processes, heat generally flows from regions with higher temperatures to those with lower temperatures until thermal equilibrium is reached. Larger bodies of water with larger temperature gradients exhibit a consistent heat flow toward the lower temperature region. However, due to the low thermal inertia of the water mass in the MSS–SS, thermal equilibrium was rapidly attained, indicating that the SW reached its heat-absorbing capacity. Consequently, there was a higher heat transfer rate to the surroundings, especially for an uninsulated condensing tower (Shatat & Mahkamov, 2010). Due to the intermittent nature of solar radiation, Fig. 10 also illustrates that the condensing tower's thermal efficiency fluctuated throughout the day. It increased to 9.03% at 1 PM, decreased to 6.41%, rose to 8.04%, and finally decreased to 2.4% later in the day. The varying intensities of solar radiation influenced these fluctuations. Figure 3 indicates that the evaporator was not generating sufficient vapour and injecting it into the stages, resulting in increased internal heat losses from the insulated condensing tower. The hourly thermal efficiency profile behaved similarly across the experimental tests on days with low solar intensity.

Moreover, for November 12, 2020, the hourly thermal efficiency showed a consistent rise from the lowest point of 19.6% to a peak of 51.67% at 3 PM. These observations suggested increased heat losses during periods of high solar intensity or when the condensing tower received insufficient heat input, leading to internal losses. On November 12, 2020, the thermal efficiency increased later in the day to a maximum of 68.71%. There was a rapid decline in solar radiation (as shown in Fig. 3) around 3 PM, coinciding with the reduction in the heat

input rate. The analysis indicated that the condensing tower operated optimally with reduced heat input rates, typically around 600 W/m^2 or in an impulsive mode during periods of high solar intensity.

Figure 11 illustrates the hourly thermal efficiency of the ETSCs computed from Eqs. 1 and 2. The efficiency curves reveal that as solar intensity increased from the morning, the efficiency also increased, reaching its peak at 79.22% and 79.9% on November 12, 2020, and June 26, 2021, respectively. Figure 11, in conjunction with Fig. 3, suggests that the collection efficiency was optimised before the peak solar radiation was achieved on both days. Beyond this point, any additional increase in the rate and heat intensity contributed to losses to the surrounding environment.

On November 12, 2020, the ETSCs' efficiency remained relatively stable, hovering around 70% for most of the day, declining later as solar radiation decreased (Fig. 3). Conversely, on June 26, 2021, the efficiency started to fall earlier due to low solar intensity, which affected the rate of heat input into the system.

Figure 3, in conjunction with Figs. 10 and 11, also reveals that the solar radiation curves for both days reached approximately 600 W/m^2 at the same time when the collection efficiencies peaked. This indicates that maintaining a controlled rate of heat input, hovering around 600 W/m^2 , or adopting an impulsive mode during periods of higher solar intensity could be advantageous in reducing heat losses to the surroundings and enhancing the system's thermal efficiency.

The efficiency curve for June 26, 2021, further suggests that most of the distillate was produced earlier in the day, before 1 PM. This is evident due to the sharp decline in solar radiation (Fig. 3), increased wind velocity (Fig. 7), and a very low ambient air temperature (Fig. 8) occurring later in the day. The combination of these factors was unfavourable for the desalination process during that time.

The highest distillate production from the entire desalination system occurred when the average solar radiation (585 W/m^2) and wind velocity (3.12 m/s) were elevated. The study established a strong connection between the increased insolation, which boosted the evaporation rate, and the higher wind velocity, which efficiently cooled and condensed the vapour. Furthermore, because most of the distillate was generated during daylight hours, the impact of ambient air temperature was deemed not to be as influential compared to solar radiation and wind velocity on these 2 days (November 12, 2020, and January 13, 2021). However, the same was not true during off-sunshine hours, as demonstrated in Figs. 4, 5 and 6.

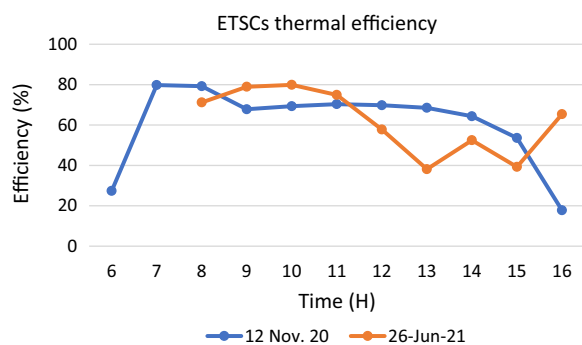


Fig. 11 ETSCs hourly thermal efficiency

When examining the five stacked stages (excluding the BSS), it was observed that they produced the same amount of distillate, measuring 6730 ml, on both November 12, 2020, and January 13, 2021. This finding indicated that further increases in the averaged heat input rate did not correlate with increased distillate output. As mentioned earlier, any increments beyond 600 W/m² (not averaged) resulted in thermal damage conditions and increased heat transfer to the surroundings.

A noteworthy correlation was established between wind velocity and thermal efficiency for the dates mentioned (November 12, 2020, and January 13, 2021). A low average wind velocity of 1.54 m/s allowed for higher preheating of the secondary tank SW, leading to prolonged thermal energy storage and continued desalination. In contrast, the averaged wind velocity of 3.12 m/s rapidly cooled the condensing tower, resulting in the same distillate production on these 2 days despite a minor difference of 3.2 W/m² in solar radiation.

Error data

In the analysis of overall thermal efficiency, condensing tower thermal efficiency, and ETSCs thermal efficiency, errors were encountered during specific times of the day. These errors occurred early morning and as solar radiation diminished toward sunset. The analysis produced erroneous results, including negative or small values or unreasonably large values. These errors were attributed to the very low rate of thermal energy input for both the condensing tower and overall thermal efficiency calculations. They did not align with the assumptions of an equal hourly distillate production, which led to overestimating the heat input required to produce the distillate.

Furthermore, while errors were observed in the ETSCs thermal efficiency calculations, there was also a significant drop in solar radiation during the summer on a sloped surface, as considered in the numerical estimation. The orientation of the ETSCs relative to the sun could have influenced the solar incidence angle, thereby reducing the heat flux onto the surface of the ETSCs (Tiwari & Tiwari, 2007).

Conclusion

The study demonstrated the potential for heat recovery in a vapour-based MSS–SS. The findings indicated that the heat generated can be effectively reused without thermal energy storage materials. There was 22.42% overall thermal efficiency enhancement due to an increased average heat input rate of 375.19 W/m² from 209.81 W/m². Contrarily, a further increase from 28.31% by 5.52% with a decline of 3.2 W/m² from 585 W/m². Notably, the wind velocity and ambient air temperature directly influenced

the desalination with solar radiation as the main force. For wind velocity at 3.2 m/s and a heat rate of 585 W/m², the SW was preheated maximally to 66.8 °C. With 1.54 m/s and 581.81 W/m², the SW reached 75.5 °C. However, the preheated SW (75.5 °C) declined to within 0.2 °C difference from 66.8 °C after sunset, emphasising the complex nature of the wind and ambient air temperature contributions to the desalination process. This was primarily due to heightened heat loss to the environment resulting from a rapid decline in ambient air temperature. Therefore, the comprehensive analysis underscores the importance of balancing various contributing factors for optimal operation.

Furthermore, it was observed that the highest overall distillate output correlated with increased cooling by wind velocities, reaching the average of 3.12 m/s. However, for the five stacked stages (excluding the BSS), the distillate output was the same for the average solar radiation of 585 W/m² or 581.8 W/m². This suggested no discernible correlation between the distillate yield and a further increase in heat input rate from 581.8 W/m². Conversely, the SW preheating increased for a low average wind velocity of 1.54 m/s, enhancing overall thermal efficiency.

With its current configuration, the MSS–SS exhibited an overall daily thermal efficiency ranging from 0% to 33.83%. Meanwhile, the condensing tower's maximum hourly thermal efficiencies were 68.71% and 34.1% for the spring and winter, respectively. In the spring season, the maximum thermal efficiency values corresponded with a rapidly declining heat input rate approaching a peak of ~600 W/m² later in the day. Therefore, an approximate heat input rate of 600 W/m² (not averaged) with the total isolation of external environmental elements could be suitable for optimal operation, and an impulsive mode could be adapted for high solar intensities.

For future work, an attempt should be made to isolate the environmental elements, increase the SW body mass, and feed the thermal energy steadily. Scaling down the ETSC size will reduce the CBA ratio while preventing thermal damage.

Abbreviations

Acronyms

BSS	Basin solar still
CBA	Collector-to-basin area
CPL	Cost per litre
CSS	Conventional solar still
ETSC	Evacuated tube solar collector
MSS–SS	Multistage solar still–stacked stages
OD	Outside diameter
PCM	Phase change material
SW	Saline water
SP	Solar panel
ET	Equation of time

ST Solar time
 LT Local time

List of symbols

\dot{Q}_{ETSC}	Collected heat energy (W/m^2)
\dot{Q}_{loss}	Total heat loss to the environment (W/m^2)
\dot{q}_{losses}	Heat loss per stage (W/m^2)
\dot{Q}_{evap}	Evaporative energy (W/m^2)
T_a	Ambient air temperature ($^{\circ}C$)
T_m	SW average temperature ($^{\circ}C$)
T	Temperature ($^{\circ}C$)
I_{sc}	Solar constant (W/m^2)
I_H	Total hourly solar radiation on a horizontal surface (W/m^2)
I_b	Hourly beam solar radiation on a horizontal surface (W/m^2)
I_d	Hourly diffuse solar radiation on a horizontal surface (W/m^2)
I_{β}	Total hourly solar radiation on an inclined surface (W/m^2)
$I_{b\beta}$	Hourly beam solar radiation on an inclined surface (W/m^2)
$I_{d\beta}$	Hourly diffuse solar radiation on an inclined surface (W/m^2)
I_r	Hourly ground reflected solar radiation (W/m^2)
ω	Hour angle (h, min)
ω_i	Hour angle 1 (h, min)
ω_{ii}	Hour angle 2 (h, min)
θ	Solar radiation incidence angle ($^{\circ}$)
θ_z	Zenith angle ($^{\circ}$)
φ	Latitude of the location ($^{\circ}$)
E_o	Eccentricity factor
ρ_g	Ground reflectance
ρ_o	Extra-terrestrial radiation (MJ/m^2 h)
R_b	Beam tilt factor
t_d	Time duration (h, min)
δ	Declination angle ($^{\circ}$)
L_s	Standard meridian for local zone
L_{loc}	Longitude for local location ($^{\circ}$)
S_c	Seasonal correlation factor
ρ	Density (kg/m^3)
k_d	Hourly diffuse fraction
η	Efficiency (%)
\dot{m}_{sw}	SW mass flow rate (kg/s)
cp	Specific heat capacity (kJ/kg $^{\circ}C$)
\dot{m}_e	Vapour mass flow rate (kg/s)
hf_g	Evaporative energy (kJ/kg)
f_{Hay}	Hay's anisotropic index
M_f	Hourly clearness index
n	Number of a day in a year

Subscript

1	Stage 1
2	Stage 2
3	Stage 3
4	Stage 4
5	Stage 5
Dist.	Distillate
e	Evaporation
Evap.	Evaporator
s	Condensing surface
d	Diffuse
β	Inclined surface angle
Hay	Hay's model
z	Zenith
b	Beam
g	Ground

Acknowledgements

The authors would like to thank the National Research Foundation for its financial support.

Author contributions

The corresponding author (MMM) performed the experiments, data gathering, and the manuscript write-up. The co-author (VM) substantively revised the work.

Funding

The National Research Foundation funded this work as a research grant.

Data availability

The data sets generated and analysed during the current study are available in the [Cape Peninsula University of Technology, Esango] repository, https://esango.cput.ac.za/articles/dataset/Development_of_vapour_based_multi_stage_solar_still_desalination_system_/19475981.

Declarations

Competing interests

The authors declare that they have no competing interests.

Received: 20 August 2023 Accepted: 8 November 2023

Published online: 24 November 2023

References

- Abd Elbar, A. R., & Hassan, H. (2020). Enhancement of hybrid solar desalination system composed of solar panel and solar still by using porous material and saline water preheating. *Solar Energy*, 204, 382–394.
- Aboabboud, M. M., Horvath, L., Szépvölgyi, J., Mink, G., Radhika, E., & Kudish, A. I. (1997). The use of a thermal energy recycle unit in conjunction with a basin-type solar still for enhanced productivity. *Energy*, 22(1), 83–91.
- Chen, Y., Ji, X., Lv, G., Jia, Y., Yang, B., & Han, J. (2023). Study on compound parabolic concentrating vaporized desalination system with preheating and heat recovery. *Energy*, 276, 127619.
- Chen, Z., Peng, J., Chen, G., Hou, L., Yu, T., Yao, Y., & Zheng, H. (2017). Analysis of heat and mass transferring mechanism of multi-stage stacked-tray solar seawater desalination still and experimental research on its performance. *Solar Energy*, 142, 278–287.
- Diez, F. J., Martínez-Rodríguez, A., Navas-Gracia, L. M., Chico-Santamarta, L., Correa-Guimaraes, A., & Andara, R. (2021). Estimation of the hourly global solar irradiation on the tilted and oriented plane of photovoltaic solar panels applied to greenhouse production. *Agronomy*, 11(3), 495.
- Fallahzadeh, R., Aref, L., Avargani, V. M., & Gholamirajenaki, N. (2020). An experimental investigation on the performance of a new portable active bubble basin solar still. *Applied Thermal Engineering*, 181, 115918.
- Kaushal, A. K., Mittal, M. K., & Gangacharyulu, D. (2017). Productivity correlation and economic analysis of floating wick basin type vertical multiple effect diffusion solar still with waste heat recovery. *Desalination*, 423, 95–103.
- Khalilmoghdam, P., Rajabi-Ghahnavieh, A., & Shafiq, M. B. (2021). A novel energy storage system for latent heat recovery in solar still using phase change material and pulsating heat pipe. *Renewable Energy*, 163, 2115–2127.
- Koffi, P. M. E., Andoh, H. Y., Gbaha, P., Touré, S., & Ado, G. (2008). Theoretical and experimental study of solar water heater with internal exchanger using thermosiphon system. *Energy Conversion and Management*, 49(8), 2279–2290.
- Liu, Z. H., Hu, R. L., & Chen, X. J. (2014). A novel integrated solar desalination system with multi-stage evaporation/heat recovery processes. *Renewable Energy*, 64, 26–33.
- Mbadanga, P. J. K. (2015). *A solar water purification system for rural areas*. Doctoral dissertation, Cape Peninsula University of Technology (pp. 49–51).
- Mdletshe, Z., Msomi, V., & Nemraoui, O. (2023). Solar water heating based on Bellville weather conditions in winter. *Renewables: Wind, Water, and Solar*, 10(1), 1–10.
- Mkhize, M. M., & Msomi, V. (2022). An experimental investigation of the novel standalone vapour-based multistage solar still with stacked stages. *Desalination and Water Treatment*, 276, 40–49.
- Mkhize, M. M., & Msomi, V. (2023). Year-round experimental analysis of the productivity of vapour-based multistage solar still: A developmental study. *Journal of Renewable Energy*, 2023, 1–15.
- Mousavi Maleki, S. A., Hizam, H., & Gomes, C. (2017). Estimation of hourly, daily and monthly global solar radiation on inclined surfaces: Models re-visited. *Energies*, 10(1), 134.

- Özcan, Y., & Deniz, E. (2023). Solar thermal waste heat energy recovery in solar distillation systems by using thermoelectric generators. *Engineering Science and Technology, an International Journal*, 40, 101362.
- Pangwa, N., & Msomi, V. (2022). Progress made in eliminating factors affecting solar stills productivity. *Materials Today: Proceedings*, 57, 969–974.
- Rajaseenivasan, T., Tinnokesh, A. P., Kumar, G. R., & Srithar, K. (2016). Glass basin solar still with integrated preheated water supply—theoretical and experimental investigation. *Desalination*, 398, 214–221.
- Schwarzer, K., da Silva, E. V., Hoffschmidt, B., & Schwarzer, T. (2009). A new solar desalination system with heat recovery for decentralised drinking water production. *Desalination*, 248(1–3), 204–211.
- Sharshir, S. W., Farahat, M. A., Joseph, A., Kandeal, A. W., Rozza, M. A., Abou-Taleb, F., Kabeel, A. E., & Yuan, Z. (2023). Comprehensive thermo-enviroeconomic performance analysis of a preheating-assisted trapezoidal solar still provided with various additives. *Desalination*, 548, 116280.
- Shatat, M. I., & Mahkamov, K. (2010). Determination of rational design parameters of a multi-stage solar water desalination still using transient mathematical modelling. *Renewable Energy*, 35(1), 52–61.
- Tiwari, A. K., & Tiwari, G. N. (2007). Annual performance analysis and thermal modelling of passive solar still for different inclinations of condensing cover. *International Journal of Energy Research*, 31(14), 1358–1382.
- Zhu, Z., Wang, Q., Li, Z., Chen, M., Wang, L., & Zheng, H. (2022). Performance research and comparison of integrated passive solar-concentrated stills buried in soil: With/without heat recovery. *Energy Conversion and Management*, 256, 115400.

Publisher's Note

Springer Nature remains neutral with regard to jurisdictional claims in published maps and institutional affiliations.

Submit your manuscript to a SpringerOpen[®] journal and benefit from:

- ▶ Convenient online submission
- ▶ Rigorous peer review
- ▶ Open access: articles freely available online
- ▶ High visibility within the field
- ▶ Retaining the copyright to your article

Submit your next manuscript at ▶ [springeropen.com](https://www.springeropen.com)
